Earthquakes and Structures, *Vol. 14, No. 4 (2018) 337-347*
DOI: https://doi.org/10.12989/eas.2018.14.4.337

Seismic response of steel reinforced concrete spatial frame with irregular section columns under earthquake excitation

Jianyang Xue*, Chaofeng Zhou[a], Zuqiang Liu[b] and Liangjie Qi[c]

College of Civil Engineering, Xi'an University of Architecture and Technology, Xi'an, China

(Received March 25, 2017, Revised February 27, 2018, Accepted March 2, 2018)

Abstract. This paper presents some shaking table tests conducted on a 1/4-scaled model with 5-story steel reinforced concrete (SRC) spatial frame with irregular section columns under a series of base excitations with gradually increasing acceleration peaks. The test frame was subjected to a sequence of seismic simulation tests including 10 white noise vibrations and 51 seismic simulations. Each seismic simulation was associated with a different level of seismic disaster. Dynamic characteristic, strain response, acceleration response, displacement response, base shear and hysteretic behavior were analyzed. The test results demonstrate that at the end of the loading process, the failure mechanism of SRC frame with irregular section columns is the beam-hinged failure mechanism, which satisfies the seismic code of "strong column-weak beam". With the increase of acceleration peaks, accumulated damage of the frame increases gradually, which induces that the intrinsic frequency decreases whereas the damping ratio increases, and the peaks of acceleration and displacement occur later. During the loading process, torsion deformation appears and the base shear grows fast firstly and then slowly. The hysteretic curves are symmetric and plump, which shows a good capacity of energy dissipation. In summary, SRC frame with irregular section columns can satisfy the seismic requirements of "no collapse under seldom earthquake", which indicates that this structural system is suitable for the construction in the high seismic intensity zone.

Keywords: steel reinforced concrete (SRC); spatial frame; irregular section column; shaking table test; seismic response

1. Introduction

Steel reinforced concrete (SRC) irregular section columns structure is a new type of structure, which is the combination of irregular section columns structure and steel reinforced concrete structure. It has much evident superiority. That the width of the column is equal to the in-filled wall makes better use of available space, and improves the esthetic appearance of structure. It also has some other advantages, such as high bearing capacity, good seismic performance (Chen *et al.* 2013, Liu *et al.* 2012, Zhou *et al.* 2012, Zhang *et al.* 2016). With the appearance of SRC irregular section columns, the application of irregular section column structure is expanded, especially the application in the high seismic zone.

At present, researches on SRC irregular section column structure mainly focus on the components and joints (Chen *et al.* 2014, 2015, 2016, Deng *et al.* 2010, Tokgoz and Dundar 2012, Xue *et al.* 2011, 2012, Xu *et al.* 2014a, 2014b, Wang *et al.* 2010). As for researches on the overall structure, Yang *et al.* (2009, 2015) presented some experimental studies on a one-bay and two-story plane frame with 1/2 scale which consists of RC beams and T-shaped SRC columns, and Xue *et al.* (2014, 2016) and Liu *et al.* (2014) performed some experimental studies on three 1/2.5-scaled plane frames with two-bay and three-story under low cyclic repeated loading. They made a preliminary understanding of the monolithic seismic performance of the SRC frame with irregular section columns. Their researches show that the structural system has a reasonable failure mechanism and good seismic performance, and can meet the earthquake fortification requirements. However, all the researches mentioned above only presented some static tests on SRC plane frame with irregular section columns, which obviously cannot accurately reveal the seismic performance of spatial frame under earthquake. Furthermore, after the Wenchuan earthquake, the Chinese Government pays more attention to the seismic performance of building structures. In order to get a further practical application in construction for SRC irregular section columns structure, it is urgent for researchers to study the seismic performance of its spatial frame structure under real earthquake. However, at present there is no study on the shaking table tests of SRC spatial frame with irregular section columns. Shaking table tests play an important role in studying seismic responses and failure mechanism of targeted structure, and are one of the important methods to study and evaluate the seismic performance of structures (Magenes *et al.* 2010, Ceccotti *et al.* 2013, Furukawa *et al.* 2013, Lu *et al.* 2007). In order to research the overall structural seismic response under earthquake, this paper presents a detailed shaking table test

*Corresponding author, Professor
E-mail: jianyang_xue@163.com
[a]Ph.D. Candidate
E-mail: zhouchaofeng163@163.com
[b]Associate Professor
E-mail: liuzuqiang0081@126.com
[c]Ph.D. Candidate
E-mail: qiliangjie@gmail.com

http://www.techno-press.com/journals/eas&subpage=7
ISSN: 2092-7614 (Print), 2092-7622 (Online)

of scaled model on SRC spatial frame with irregular section columns. The paper aims to provide some insights into the overall dynamic behavior of the new structural system and analyze its seismic responses.

2. Experimental program

2.1 Description of the shaking table

The shaking table with three-dimensional and six degree-of-freedom can bear maximum payload of 2500 kg with dimensions of 4000 mm×4000 mm in the civil engineering laboratory of the Xi'an University of Architecture and Technology. It can vibrate with two maximum horizontal accelerations of 1.5 g and 1.0 g, with a maximum vertical acceleration of 0.7 g. Its frequency ranges from 0.1 to 50 Hz and 74 channels can be used to obtain data during testing procedure. The data acquisition system can record 100 data per second.

2.2 Test specimen and material properties

Under the background of seismic design intensity 8 and Type-II site, a structure prototype of two-span and five-story spatial frame was designed. Its span and deep both are 4000 mm, and story heights equal to 3600 mm and 3000 mm for the first and the other stories. Considering the size and bearing mass of the shaking table, the model had to be geometrical scaled down by 1/4 scale. Steel elements and reinforced concrete elements were modeled with steel and fine-aggregate concrete, respectively. Therefore, the elastic modulus scaling parameter for material was chosen as 1. Under the condition of full weight, the horizontal acceleration scaling parameter was chosen as 1 in order to accurately simulate the earthquake. Subsequently, other scaling parameters can be expressed in terms of the basic parameters mentioned above. The scaling parameters are given in Table 1. According to the similitude law, the mass of every component can be calculated. So the mass of the 1st storey was about 1.38t and the mass of every storey (except for 1st storey) was about 1.15t. The artificial mass was applied through pouring four concrete cube blocks with the dimension of 600 mm×600 mm×450 mm on each storey, and the mass of each cube block was 0.4t. The total mass of the model without the foundation beam was about 14t.

The scale structure is a symmetrical model with a 田-

Table 1 Similitude scale parameters

Parameter	Similitude relationship	Scaling coefficient
S_l	S_l	1/4
S_a	S_a	1
S_E	S_E	1
S_t	$S_t=\sqrt{S_l}$	1/2
S_m	$S_m=S_E \bullet S_l^2$	1/16
S_ε	$S_\varepsilon=S_E$	1
S_σ	$S_\sigma=S_\varepsilon \bullet S_E$	1
S_ξ	$S_\xi=S_E\sqrt{S_l^3}$	1/8

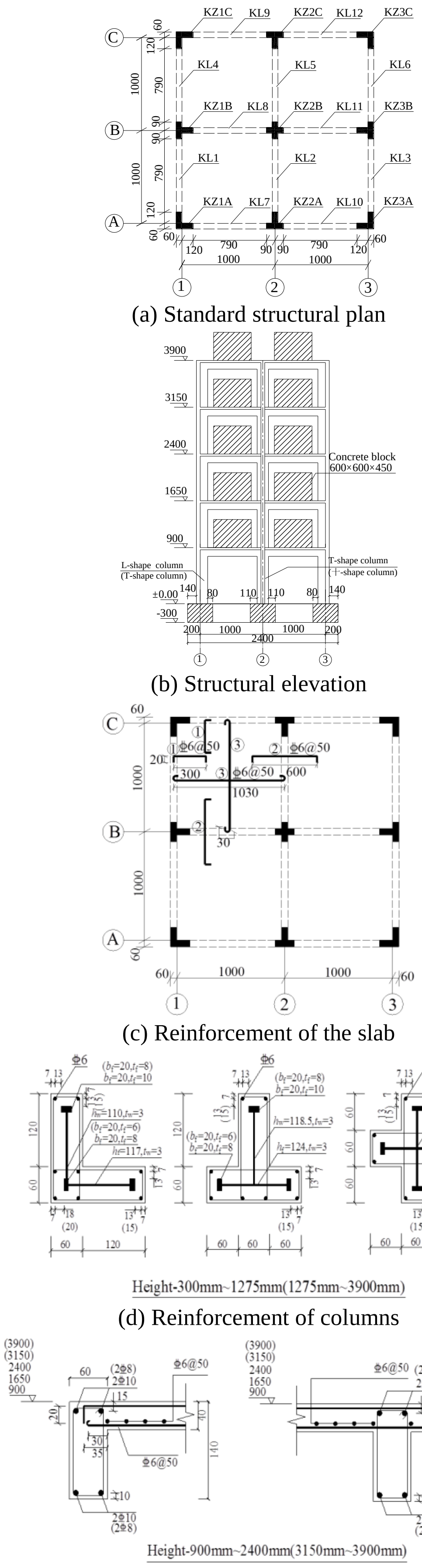

Fig. 1 Details of specimen

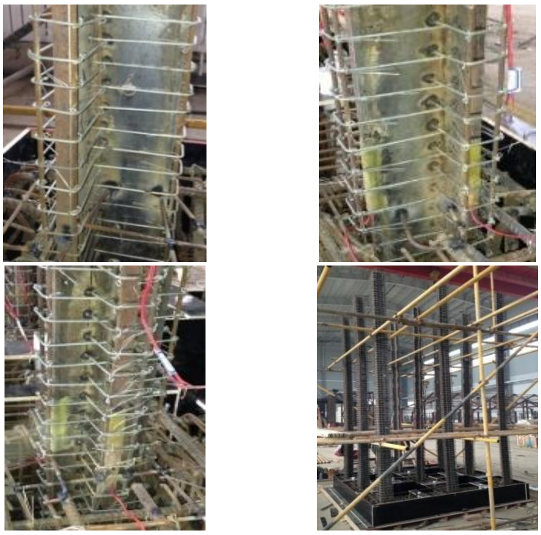

Fig. 2 Steel skeleton

Table 2 Mechanical indexes of steel

Material	Diameter (Plate thickness)	Elastic modulus E_s/GPa	Yield strength f_y/MPa	Yield strain $\varepsilon_y/10^{-6}$	Ultimate strength f_u/MPa
Steel plate	10 mm	172	396	2301	566
	8 mm	208	328	1577	477
	6 mm	209	333	1593	488
	3 mm	207	322	1553	457
Rebar	Φ10	180	530	2850	640
	Φ 8	180	488	2696	648
	Φ 6	210	392	1806	588
Iron wire	10#	200	321	1605	446

shaped foundation beams of 400 mm×300 mm, where 400 mm and 300 mm represent the width and the height, respectively. The column base is inserted into the foundation beam so as to simulate the rigid boundary condition. The height of test model is 4200 mm, where story heights equal to 900 mm and 750 mm for the first and the other stories. The scale model consists of three plane frames connected by RC beams of 140 mm×60 mm and RC slabs with the thickness of 40 mm. In the spatial frame, L-shaped column is regarded as the corner column, T-shaped column is regarded as the side column, and +-shaped column is regarded as the middle column. The ratio of the limb height to the limb thickness is 3, and the limb thickness is 60 mm. The detail geometry and steel configuration of the specimen is shown in Fig. 1, where the unit is millimeter.

The shape steel consists of welded steel plate with different thickness, and the stirrups were welded to the shape steel with U-shape or non-closed rectangular-shape, then longitudinal rebars were assembled with the stirrups. As shown in Fig. 2, the steel skeletons are manufactured. Properties of the rebar and steel plate are shown in Table 2. 15 concrete cube blocks (150 mm×150 mm×150 mm) were poured for concrete material test. Its average compression strength was measured as 34.36 MPa after curing for 28 days. To ensure an effective transmission of the table motion to the foundation of the specimen, twelve round holes were designed in foundation beams, and then the cross foundation beams were firmly fastened to the shaking table through bolt connections. Fig. 3 shows an overview of the specimen after fastened to the shaking table.

Fig. 3 Test model

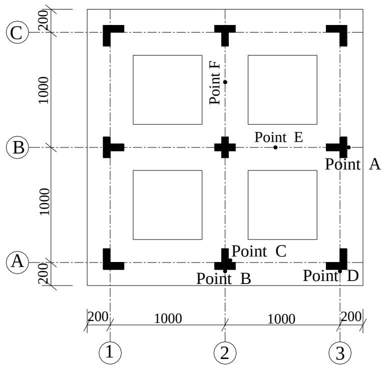

Fig. 4 The arrangement of acceleration and displacement measurement points

2.3 Sensors layout

The instrument was installed so as to capture the overall and local responses in the period of loading. In order to describe the layout of measurement points, the horizontal direction along Ⓐ (Ⓑ or Ⓒ) axis and ① (② or ③) axis were defined as X axis and Y axis, respectively, and the vertical direction was defined as Z axis.

A total of 74 data channels was recorded, where 30 channels, 12 channels, 32 channels were for acceleration measurements, displacement measurements and strain measurements, respectively. The layout of the main measurement points (except for strain gauges) is shown in Fig. 4. As shown in Fig. 4, the points A and C along the height of the structure represent accelerations in direction X, the points B and D along the height of the structure represent accelerations in direction Y, and the points E and F along the height of the structure respectively represent the displacements in direction X and Y. Fig. 5 shows the arrangement of strain measurement points, where EA, ES represent shape steel strain gauge and rebar strain gauge, respectively. Due to the limitation of the number of data channels, the strain gauges mounted on the beam end were distributed at the 1st story and 3rd story, and the others were distributed at column end of the 1st story, 2nd story and 3rd story. These strain gauges were mounted on the rebar and

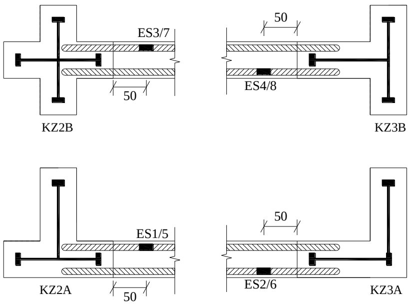

(a) The arrangement of rebar strain

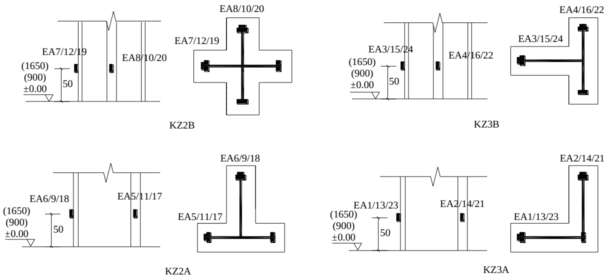

(b) The arrangement of shape steel strain

Fig. 5 The arrangement of strain measurement points

shape steel at the sections of 50 mm from each beam and column end.

2.4 Seismic loading procedure

Considering the relevant code of Seismic Design of Buildings and the spectral density properties of Type-II site soil, the three waves, including two nature waves and an artificial wave, were selected. They were El Centro wave (1940), Taft wave (1952) and Lanzhou wave. In the test, all waves were input successively by the manner of one-dimensional, two-dimensional and three-dimensional. According to the code for seismic design of building (GB 50011-2010), the factors of 0.85 and 0.65 are stipulated, namely a_x: a_y: a_z=1: 0.85: 0.65, where a_x, a_y and a_z represent the acceleration peak in direction X, Y and Z, respectively. After different series of ground acceleration were input, white noise the peak value of which is selected to 50 gal was input to determine the damped natural frequencies and the damping ratios of the model structure. Because the design seismic intensity in Xi'an is specified as 8, the test was carried out in six phases representing frequent, basic and seldom-occurred earthquakes of design seismic intensity 8 and 9, respectively. Furthermore, in order to evaluate the overall capacity of the structure, especially under extremely seldom earthquakes, the acceleration peaks of the waves were increased to 1300 gal by gradually increasing acceleration amplitudes. The test programme is listed in Table 3, where WN represents the white noise, E/T/L, EY/TY/LY and EZ/TZ/LZ represent 1-D, 2-D and 3-D wave, respectively.

3 Test results

3.1 Cracking and failure pattern

Table 3 Test programme

Run#	Input	Peak acceleration (gal)		
		Direction X	Direction Y	Direction Z
1	1WN	50	50	50
2, 3, 4	E1, T1, L1	70	—	—
5, 6, 7	EY1, TY1, LY1	70	60	—
8, 9, 10	EZ1, TZ1, LZ1	70	60	50
11	2WN	50	50	50
12, 13, 14	E2, T2, L2	140	—	—
15, 16, 17	EY2, TY2, LY2	140	120	—
18, 19, 20	EZ2, TZ2, LZ2	140	120	90
21	3WN	50	50	50
22, 23, 24	E3, T3, L3	200	—	—
25, 26, 27	EY3, TY3, LY3	200	170	—
28, 29, 30	EZ3, TZ3, LZ3	200	170	130
31	4WN	50	50	50
32, 33, 34	E4, T4, L4	400	—	—
35, 36, 37	EY4, TY4, LY4	400	340	—
38, 39, 40	EZ4, TZ4, LZ4	400	340	260
41	5WN	50	50	50
42, 43, 44	E5, T5, L5	620	—	—
45, 46, 47	EY5, TY5, LY5	620	530	—
48, 49, 50	EZ5, TZ5, LZ5	620	530	400
51	6WN	50	50	50
52, 53, 54	EZ6, TZ6, LZ6	800	680	520
55	7WN	50	50	50
56	EZ7	1000	850	650
57	8WN	50	50	50
58	EZ8	1100	930	720
59	9WN	50	50	50
60	E9	1300	—	—
61	10WN	50	50	50

The damage process of specimen under earthquake mainly shows the emergence and development of cracks on the surface, the gradual yield at the shape steel flange, web and the longitudinal bars of beam ends, and the bond slip between the shape steel and the concrete. During the loading process, the concrete cracks on the surface of the model are fully expanded, and the longitudinal bar of the beam ends and the shape steel flange successively enter into the yield stage. The specific experimental process is described as follows:

(1) The test model survived from 70 gal to 140 gal without visible damage, and only some fine cracks occurred at the beam end of the 1st story, which indicates that the structure is in the elastic stage.

(2) After inputting the seismic wave with the peak acceleration of 200 gal, a few vertical flexural cracks and oblique cracks appeared at the beam end and a few diagonal cracks extended to the top of the beam; few horizontal cracks appeared at the bottom and the top of column. Under the seismic wave with the peak acceleration of 400 gal, the seismic response of the structure was obvious. The original cracks continued to extend and a large number of new cracks were generated in the 1st story. And few fine cracks

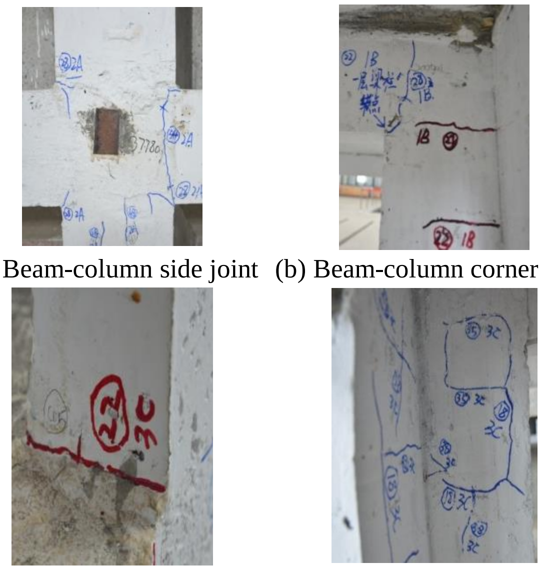

(a) Beam-column side joint (b) Beam-column corner joint

(c) Column base (d) Column center

Fig. 6 Failure patterns of the specimen

appeared at the beam end of the 2nd story.

(3) Under the seismic wave with the peak acceleration of 620 gal, the structure shook severely and the original cracks continued to expand. Bending cracks joined up at the beam end of the 1st story, and a small amount of concrete peeled. Strain tests showed that the longitudinal rebar at the beam end had been yielding and entered into the elastic-plastic stage. Horizontal cracks joined up on the column at the top and the bottom of 1st story, and a small amount of horizontal and vertical cross cracks appeared in the middle of the column at the 1st story. Few diagonal cracks at the beam-column joint of the 1st story extended to the core area of joint in the direction of 45°. The original cracks at the beam end of the 2nd story gradually extended, and a small amount of horizontal cracks appeared at the top and the bottom of column. And a few fine cracks appeared at the beam end of the 3rd story. Under the seismic wave with the peak acceleration of 800 gal, cracks at the beam end of the 1st story progressively extended, which made the plastic deformation aggravated. The horizontal joined-up cracks on column at the top and bottom of the 1st story gradually widened, the horizontal and vertical cracks in the middle of the column joined together, and cracks at the core area of joint gradually extended. The original cracks at the beam end of the 2nd and 3rd story continued to develop with a large number of new cracks and the yielding of longitudinal bar at the beam end. Horizontal cracks on column joined up at the top and bottom of the 2nd story with a few of fine cracks in the middle of the column and in the core area of the beam-column joints.

(4) Under the action of seismic wave with the peak acceleration of 1000 gal, 1100 gal and 1300 gal, the plastic deformation at the beam end of the 1st story was further aggravated, the plastic hinge was formed at the beam end and the horizontal cracks at the bottom of column were connected with the concrete peeling, and the cracks at the core area of joints of 1st story gradually extended. All the cracks at the beam end of the 2nd story were fully developed and entered into the plastic stage, the cracks at the top and the bottom of column were connected, and no obvious cracks appeared at the core area of joints. The diagonal cracks at the beam end of the 3rd story extended to the top of the beam, forming connected cracks.

In the loading process, there were fewer cracks at the 4th story and the 5th story without obvious damage. The final failure patterns are shown in Fig. 6.

Table 5 Former two dynamic characteristics of model

Input	Frequency/Hz	Damping ratio	Vibration mode
1WN	7.305	0.037	Translation of X
	8.047	0.032	Translation of Y
2WN	7.031	0.053	Translation of X
	8.047	0.044	Translation of Y
3WN	6.819	0.080	Translation of X
	7.617	0.046	Translation of Y
4WN	6.725	0.061	Translation of X
	7.305	0.051	Translation of Y
5WN	5.977	0.083	Translation of X
	6.484	0.066	Translation of Y
6WN	5.430	0.086	Translation of X
	5.977	0.065	Translation of Y
7WN	5.469	0.088	Translation of X
	5.820	0.087	Translation of Y
8WN	5.430	0.108	Translation of X
	5.547	0.111	Translation of Y
9WN	5.039	0.155	Translation of X
	5.625	0.109	Translation of Y
10WN	5.025	0.178	Translation of X
	5.468	0.114	Translation of Y

3.2 Dynamic characteristic

The model structure is scanned by the white noise at the end of each loading. After the analysis of the transfer function between the acceleration points, the damped natural frequencies of the model structures are obtained, and the corresponding damping ratios are obtained by the half-power bandwidth method, as shown in Table 5. It can be seen from the table that the first two vibration models are translational vibration. At the end of loading, the first two frequencies of the model are reduced from 7.305 Hz and 8.047 Hz to 5.025 Hz and 5.468 Hz respectively. And the first two damping ratios are increased from 0.037 and 0.032 to 0.178 and 0.114 respectively. It means that with the development of cracks and the yielding of the shape steel and rebar, the damage within the structure and residual deformation gradually increase, resulting in the damped natural frequency decreasing, the damping ratio increasing gradually, and the energy dissipation of structure increasing gradually.

3.3 Strain response

The time history curves of the strain on the longitudinal rebar and shape steel are shown in Fig. 7 and Fig. 8

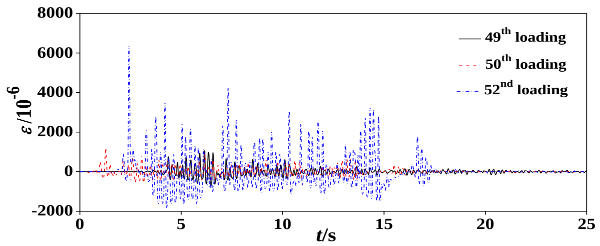

(a) the strain of point ES1

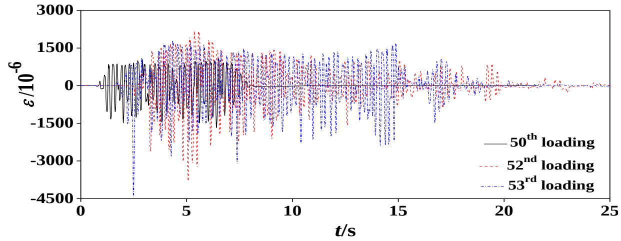

(b) the strain of point ES5

Fig. 7 Time-history curves of strain of rebars in beams

respectively. It can be seen from the figure that, in the initial loading process, the strains of the longitudinal rebar and the shape steel are in the elastic stage. In the 50th loading, the maximum strains at the point ES1 and ES5 are respectively up to 1210×10^{-6} and 1672×10^{-6}, which are close to the yielding strain of the steel. At this moment, the strain of shape steel at the bottom of column is much smaller than the yielding strain of shape steel. In the 52nd loading, the strain of the beam-end longitudinal bar increases significantly and the maximum strains at the point ES1 and ES5 are respectively up to 6419×10^{-6} and 3795×10^{-6}, which exceeds the yield strain. At this moment, the maximum strain of the shape steel at the point EA5 is up to 1144×10^{-6} and is still in the elastic stage. As the loading continues, the strains of the longitudinal bar and the shape steel gradually increase. In the 56th loading, the strain at the point EA5 is up to 2300×10^{-6} and reaches the yielding strain. In the 60th loading, the strains at the point EA1 and EA7 are respectively up to 1700×10^{-6} and 1900×10^{-6}, and these sections occur the yielding. However, the strains at the points EA11 and EA17 are respectively up to 1019×10^{-6} and 701×10^{-6}, and much smaller than the yield strain of shape steel. Generally speaking, the strain of the beam-end longitudinal rebar develops faster than that of the column-bottom shape steel, and the former occurs the yielding prior to the latter, which means that the structure can satisfy the seismic design requirements of “strong column-weak beam”.

The strain of ES1 develops faster than that of ES5, and the strain of EA5 develops faster than that of EA11 and EA17. It is shown that in the loading process, the 1st story is subjected to more seismic force than the other stories, and the section deformation of the beam end and column base section is relatively larger. It is different from the phenomenon that the plastic hinge in the quasi-static test of the SRC plane frame with irregular section columns in the literature (Liu *et al.* 2014, Xue *et al.* 2016) first appears in the middle column of top story. The reason is that the axial force of the frame column at the top story is variable

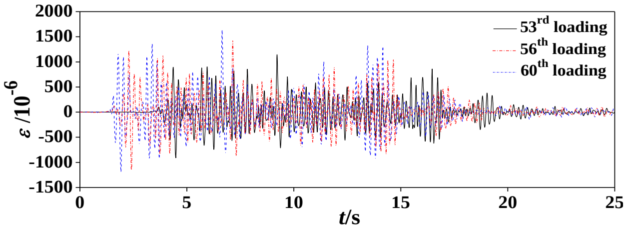

(a) the strain of point EA1

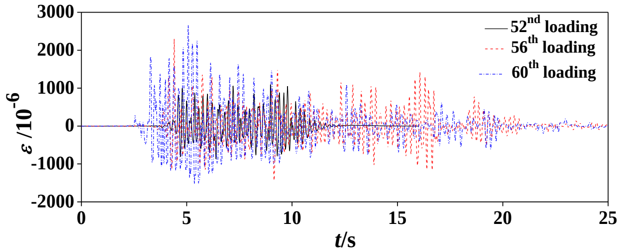

(b) the strain of point EA5

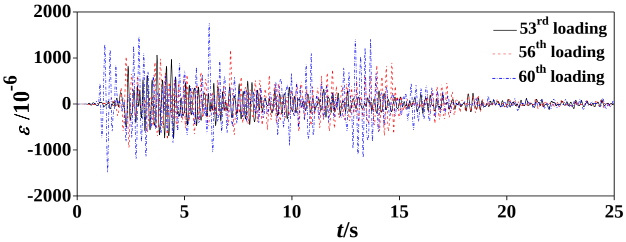

(c) the strain of point EA7

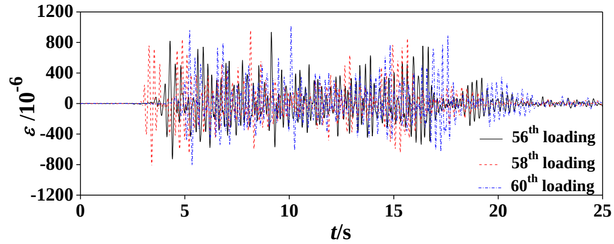

(d) the strain of point EA11

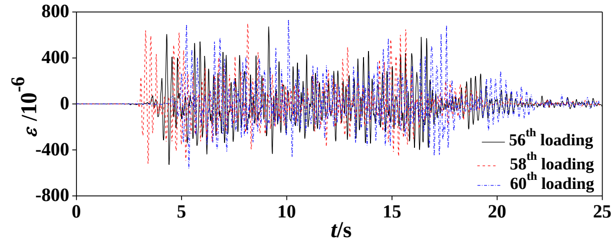

(e) the strain of point EA17

Fig. 8 Time-history curves of strain of shape steel in columns

(increase or reduce) in the shaking table test and the axial compression ratio is relatively small, so that its ductility is better. While the middle column on the top story bears larger bending moment passed by the beam end in the quasi-static test and its ductility significantly reduced under the action of large axial compression .The strain of point EA5 is larger than that of points EA1 and EA7, which indicates that the deformation of T-shaped column develops much faster than that of L-shaped column and ＋-shaped column. Compared with L-shaped and ＋-shaped column, T-shaped column is subjected to greater seismic force.

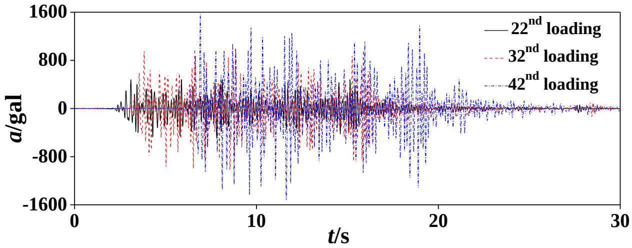

(a) Under El Centro wave with different acceleration peaks

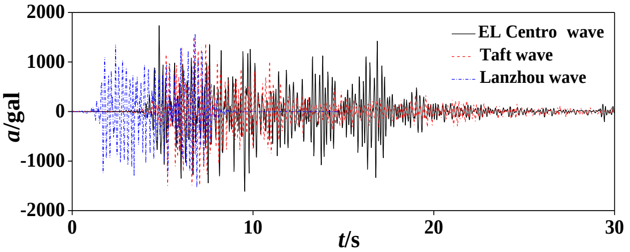

(b) Under the peak acceleration of 620 gal

Fig. 9 Time history curves of top acceleration in direction X

3.4 Acceleration response

Fig. 9 shows the acceleration response of the top story of the model in direction X. It can be seen from the figure that the peak acceleration of the top story increases with the peak acceleration of the seismic waves. As most of the components are in the elastic stage, the response curve profile is basically the same and the peak time is basically the same. With the increase of the peak acceleration of the seismic waves, the time of the acceleration response peak of the top story is postponed. The main reason is that under the sustained action of the seismic waves, the cumulative damage of the structure increases and the stiffness decreases, which affects the acceleration response of the structure. When the input acceleration peaks reach to 620 gal under different seismic waves, the acceleration responses of the top story of the structure are different. Compared with Taft wave and Lanzhou wave, the response of El Centro wave is larger than that of the Taft wave and Lanzhou wave, which indicates that the spectral response of El Centro wave has a significant influence on the dynamic response of the structure.

Fig. 10 shows the relationship between a_Y (the acceleration in direction Y) and a_X (the acceleration in direction X) of the top story of the test model. Because the structure is completely symmetrical (the center of stiffness coincides with the center of mass), the bi-directional input of the seismic wave is equivalent to the unidirectional input along a certain angle, and the a_Y-a_X curve should be a linear relationship in theory. However, the figure shows that the relationship curve is ring-shaped during the loading process. The reason may be that the time at which the components enter into the elastic-plastic stage is different from each other during the loading process and the stiffness center of the structure deviates from the mass center, resulting in the torsion deformation. Therefore, the distribution of the acceleration response is not completely along the excitation direction.

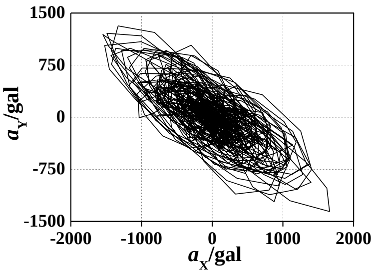

(a) The 45th loading condition

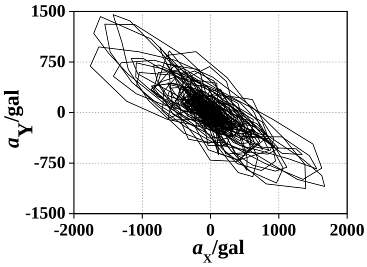

(b) The 46th loading condition

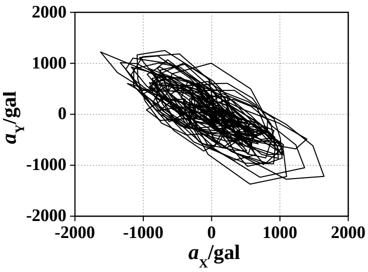

(c) The 47th loading condition

Fig. 10 Relation curves between a_Y and a_X

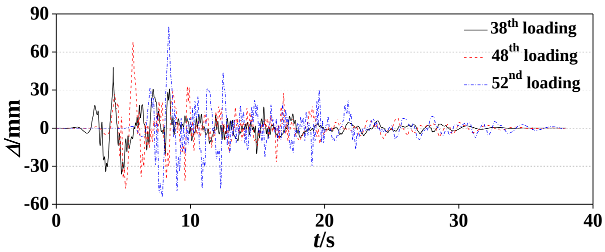

(a) Direction *X*

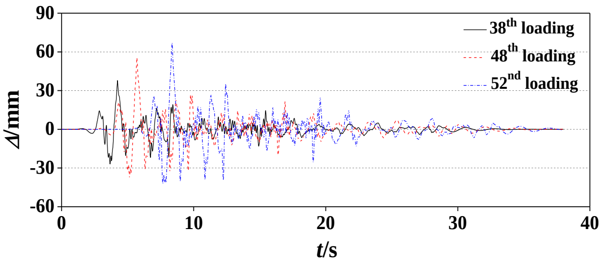

(b) Direction *Y*

Fig. 11 Time-history curves of the top displacement under El Centro wave

3.5 Displacement response

Fig. 11 shows the time history curves of displacement of the top story under El Centro wave with different acceleration peaks. It can be seen from the figure that with

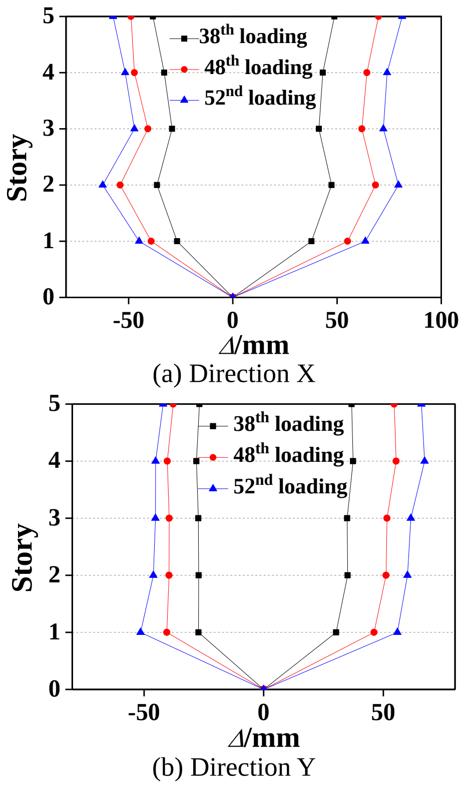

(a) Direction X

(b) Direction Y

Fig. 12 Maximum story displacement under El Centro wave

the increase of the peak acceleration, the peak displacement gradually increases in direction X and direction Y, and the time of the peak displacement is delayed.

Fig. 12 shows the displacement envelope curve of the maximum story displacement under the action of El Centro wave with different acceleration peaks. It can be seen from the figure that the positive displacement of structure is larger than the negative displacement of structure, which indicates that the degradation of the positive lateral stiffness is more serious during the loading process. The direction X is the principal earthquake direction, so the development of the damage is faster than that of direction Y, and the story displacement of direction X is larger than that of the direction Y. The overall lateral displacement curve of the direction X is S-shaped. The displacements of the 2nd and 5th stories are relatively larger, the 3rd story and the 4th story are the smallest, and the larger displacement of the 2nd story may be caused by the decrease of the steel section above the middle of the column at the 2nd story. The overall lateral displacement curve of the direction Y is generally linear and the displacement of each story is smaller.

3.6 Base shear response

According to the acceleration response and the story mass distribution, the distribution of the inter-story shear force of the model under different loading conditions can be obtained. The calculated expression is

$$F_i = \sum_{i}^{n} m_i a_i \tag{1}$$

where F_i is the shear of the i-th story; m_i is the equivalent mass of the i-th story; a_i is the acceleration of the i-th story.

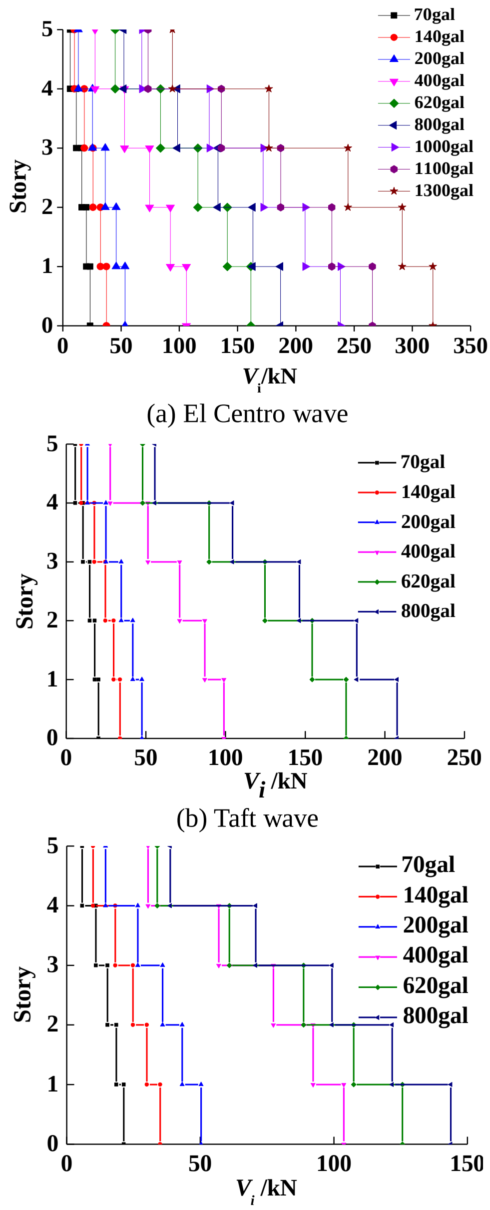

(a) El Centro wave

(b) Taft wave

(c) Lanzhou wave

Fig. 13 Distribution of the maximum inter-story shear force under different seismic waves

Fig. 13 shows the distribution of the maximum inter-story shear force under different seismic waves. It indicates that the maximum inter-story shear force shows a decrease trend along the height of structure under different seismic waves with the same acceleration peak. It can be seen from the figure that with the increase of the peak acceleration of seismic waves, the base shear of the model gradually increases. The response under El Centro wave is taken as an example to illustrate the change of base shear. During the loading process of 70 gal-620 gal, at the beginning of loading process, the structure is in the elastic stage and the stress of the longitudinal rebar and shape steel is relatively less. With the increase of the acceleration peak, the structure transits from the elastic stage to the elastic-plastic stage. The stresses of the longitudinal rebar and shape steel increase rapidly and approach yield state, which in turn produce larger base shear and make the maximum inter-story shear force close to the maximum bearing capacity. The base shear of the structure increases from 18.28 kN to 160.10 kN, the increase rate is about 700%. During the loading process from 800 gal to 1300 gal, the longitudinal rebar and the shape steel reach yield state with smaller increase of the stress, larger plastic deformation and expanding yielding area, which makes the base shear increase but decrease growth rate. The base shear increases from 227.60 kN to 317.59 kN, the increment is about 39%, and the growth slows down.

3.7 Hysteretic response

The hysteretic loop between base shear and top displacement in direction X under El Centro wave is shown in Fig. 14. It can be seen from the figure that when the input acceleration peak is no more than 400 gal, the hysteretic curve basically presents straight line and the envelope area is extremely small, and the top displacement in direction X is about 8mm. With the increase of the acceleration peak, some cracks appeared on the surface of structure, and more earthquake energy is dissipated with the development of cracks. When the acceleration peak reaches 620 gal, the top displacement in direction X is about 15 mm. Meanwhile, the longitudinal bars in beam end enter into the yield stage, and the hysteretic loop is slightly curved and begins to show non-linear features. The envelope area of the curve increases. When the acceleration peak reaches 800 gal, lots of cracks continue to develop and connect together, and a few diagonal cracks at the beam-column joint extend to the core area of joint in the direction of 45°. The hysteretic loop shows obvious non-linear features. The strain of the beam-end longitudinal bar at 1^{st} story has exceeded the yield strain of rebar while the shape steel at column base of 1^{st} story is still in elastic stage with the strain of 1144×10^{-6}. After inputting the seismic waves with the acceleration peaks of 1100 gal and 1300 gal, the shape steel in column base of 1^{st} story enters into the yield stage and the lateral stiffness of structure decreases quickly. The top displacement reaches 40 mm and the hysteretic loop becomes plumper. More energy of input seismic wave is dissipated by hysteretic energy. In the end of loading, the plastic deformation has fully developed. According to the data obtained by the displacement sensors, it can be seen that the maximum interstory drift ratios from 1^{st} story to 5^{th} story reach 1/40, 1/30, 1/28, 1/44, 1/68, respectively. Except for the 5^{th} story, the maximum interstory drift ratios of the other stories both are bigger than the limit value of the elastic-plastic interstory drift ratio stipulated in the Chinese Design Code-Technical specification for concrete structures with specially shaped columns (JG J149-2006). However, the structure has no collapse. Under the strong earthquake, the shape steel configured in columns shows the good ductility and the high bearing capacity, which makes sure that the overall structure has an excellent deformation performance.

Fig. 15 shows the cumulative hysteretic energy dissipation curve of structure under different El Centro waves. It indicates that with the increase of the acceleration

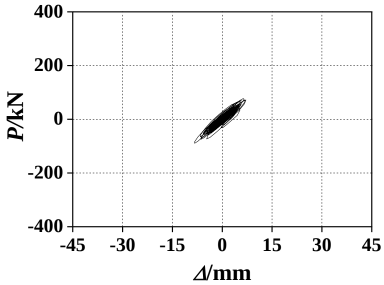

(a) Under the peak acceleration of 400gal

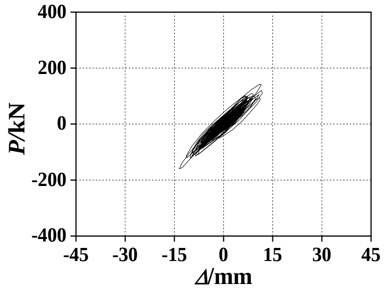

(b) Under the peak acceleration of 620gal

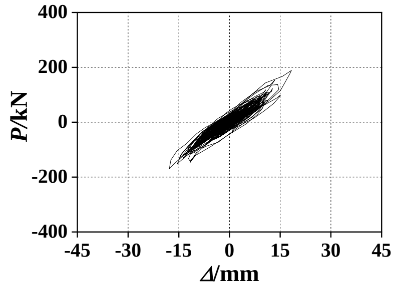

(c) Under the peak acceleration of 800gal

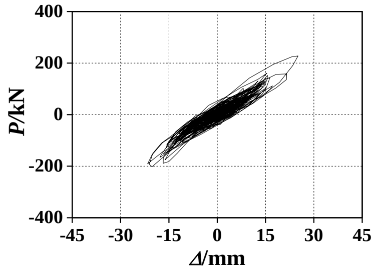

(d) Under the peak acceleration of 1100gal

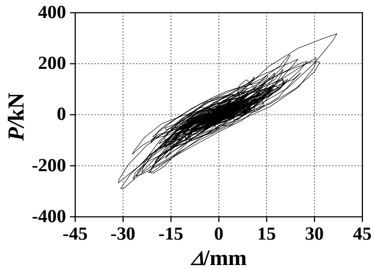

(e) Under the peak acceleration of 1300gal

Fig. 14 Hysteretic curves of base shear and top displacement under the action of El Centro wave

peak, the hysteretic energy of structure gradually increase and more earthquake energy is absorbed and dissipated. The cumulative hysteretic energy of structure is rapidly increased with stepped characteristic. In the initial loading process, the structure is in elastic stage and Hysteretic

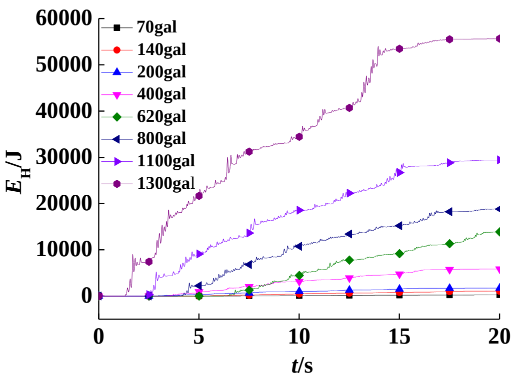

Fig. 15 The cumulative hysteretic energy dissipation curve of structure under El Centro wave

energy consumption is mainly based on recoverable elastic deformation energy. When some components of the structure enter into the yield stage, the residual deformation energy accounts for the majority of hysteretic energy dissipation, and there is a large increase of energy dissipation in a very short time. With the increase of the acceleration peak, the cumulative damage degree is further aggravated, the time required for the structure to enter the plastic stage is less, and the time when hysteretic energy dissipation curve has a large increase is advanced.

4. Conclusions

Based on the shaking table test of the 5-story SRC spatial frame with irregular section columns, the main conclusions are as follows:

• Under the action of strong earthquakes, the beam end at the 1st layer enters into the yield stage, followed by the second and third beam end. When the acceleration peak reaches 1000 gal, the shape steel of T-shaped firstly yield. The frame beam starts to yield before the frame column, which forms the typical beam-hinge failure mechanism, which meets the seismic design of strong column and weak beam. The performance of the T-shaped side column is worse than that of the +-shaped middle column and the L-shaped corner column.

• In the early loading process, the concrete gradually cracks, which leads to the slight decrease of damped natural frequencies. With the increase of the acceleration peak, the plastic deformation gradually increases and a small amount of rebar yield, which indicates that the structure enters into the elastoplastic stage. In the later loading process, the shape steel in the column base also yields. The cumulative damage rapidly aggravates so that the lateral stiffness drops fast. Therefore, the damped natural frequency of the structure always decreases and the damping ratio of the model structure gradually increases during the loading process. The first two modes of the model vibration are dominated by translational modes.

• The acceleration and displacement response of the model structure increase with the increase of the peak acceleration of the seismic waves, and the time arriving at the peak appears to be postponed.

• In the two-dimensional input seismic waves, the relationship curves between a_Y and a_X at the top story show ring-shaped features. It indicates that when the structure gradually enters into the plastic stage, there will be torsional deformation. Therefore, the acceleration response is not entirely along the excitation direction distribution.

• With the increase of the acceleration peak, the inner damage of structure gradually becomes aggravated. The increasing rate of the base shear of the model structure is much slower than that of the later time, and the hysteretic curve gradually becomes plump. The hysteretic energy dissipation of structure shows a dramatic increase, which indicates that more seismic energy is dissipated.

Acknowledgements

The authors would like to thank the National Natural Science Foundation of China (Granted No.51308444 and Granted No.50978217), Shaanxi Natural Science Foundation (Granted No.2014JQ7288), Innovation Team Project and Youth Technology Fund of Xi'an University of Architecture and Technology (Granted No.QN1408).

References

Ceccotti, A., Sandhaas, C., Okabe, M., Yasumura, M., Minowa, C. and Kawai, N. (2013), "SOFIE project-3D shaking table test on a seven-storey full-scale cross-laminated timber building", *Earthq. Eng. Struct. Dyn.*, **42**(13), 2003-2021.

Chen, Z.P., Wang, N., Zhong, M., Xue, J.Y. and Su, Y.S. (2013), "Experimental study and finite element analysis on normal section bearing capacity of steel reinforced concrete special-shaped columns", *J. Build. Struct.*, **34**(10), 108-119.

Chen, Z.P., Xu, J.J. and Chen, Y.L. (2016), "Axial compression ratio limit values for steel reinforced concrete (SRC) special-shaped columns", *Steel Compos. Struct.*, **20**(2), 295-316.

Chen, Z.P., Xu, J.J. and Xue, J.Y. (2014), "Experimental investigation on hysteretic behaviour of planar and 3D joints in cruciform SRC column frame", *J. Build. Struct.*, **35**(8), 80-87.

Chen, Z.P., Xu, J.J. and Xue, J.Y. (2015), "Hysteretic behavior of special-shaped columns composed of steel and reinforced concrete (SRC)", *Earthq. Eng. Eng. Vib.*, **14**(2), 329-345.

Deng, Z.H., Tang, G.X. and Xiang, P. (2010), "Experimental study on seismic behavior of SRC T-shaped column joints under low cyclic reversed loading", *Indus. Constr.*, **40**(6), 44-48.

Furukawa, S., Sato, E., Shi, Y., Becker, T. and Nakashima, M. (2013), "Full-scale shaking table test of a base-isolated medical facility subjected to vertical motions", *Earthq. Eng. Struct. Dyn.*, **42**(13), 1931-1949.

Liu, Z.Q., Xue, J.Y. and Zhao, H.T. (2014), "Cyclic test for solid steel reinforced concrete frames with special-shaped columns", *Earthq. Struct.*, **7**(3), 317-331.

Liu, Z.Q., Xue, J.Y., Zhou, P. and Zhao, H. (2012), "Quasi-static test and finite element analysis on solid-web steel reinforced concrete exterior frame with special-shaped columns", *J. Build. Struct.*, **33**(8), 23-30.

Lu, X.L., Zou, Y., Lu, W.S. and Zhao, B. (2007), "Shaking table model test on shanghai world financial center tower", *Earthq. Eng. Struct. Dyn.*, **36**(4), 439-457.

Magenes, G., Penna, A. and Galasco, A. (2010), "A full-scale shaking table test on a two-storey stone masonry building", *Proceedings of the14th European Conference on Earthquake Engineering*.

Tokgoz, S. and Dundar, C. (2012), "Test of eccentrically loaded L-shaped section steel fibre high strength reinforced concrete and composite columns", *Eng. Struct.*, **38**(5), 134-141.

Wang, T.C., Zhang, X.H. and Zhao, H.L. (2010), "Experimental research on seismic behavior of exterior joints with specially shaped columns reinforced by fiber", *Indus. Constr.*, **40**(1), 46-50.

Xu, J.J., Chen, Z.P. and Xue, J.Y. (2014b), "Earthquake damage evolution and influence factor analysis on space joints for T-shaped SRC column-steel beams", *J. Basic Sci. Eng.*, **22**(6), 1165-1176.

Xu, J.J., Chen, Z.P., Chen, Y.L. and Xue, J.Y. (2014a), "Seismic performance and quantitative indexes for SRC special-shaped columns", *Chin. Civil Eng. J.*, **47**(12), 133-138.

Xue, J.Y, Qi, L.J., Gao, L. and Liu, Z.Q. (2016), "Mechanical behavior of lattice steel reinforced concrete inner frame with irregular section columns under cyclic reversed loading", *Eng. Struct.*, **128**, 225-236.

Xue, J.Y., Chen, Z.P., Zhao, H.T., Gao, L. and Liu, Z.Q. (2012), "Shear mechanism and bearing capacity calculation on steel reinforced concrete irregular section columns", *Steel Compos. Struct.*, **13**(5), 473-487.

Xue, J.Y., Gao, L. and Liu, Z.Q. (2014), "Experimental study on mechanical performances of lattice steel reinforced concrete inner frame with irregular section columns", *Steel Compos. Struct.*, **16**(3), 253-267.

Xue, J.Y., Liu. Y. and Chen, Z.P. (2011), "Experimental study of the bearing capacity of steel reinforced concrete special-shaped column-beam joint", *Chin. Civil Eng. J.*, **44**(5), 41-48.

Yang, T. and Zhang, X.D. (2009), "Research on seismic behavior of frame with T-shaped SRC columns", *J. Civil Arch. Environ. Eng.*, **31**(2), 33-37.

Yang, T., Zhang, X.D. and Zhong, H.N. (2015), "Pseudo-dynamic test on seismic behaviour of frame with T-shaped SRC columns", *J. Central South Univ. (Sci. Technol.)*, **46**(6), 2171-2177.

Zhang, S., Chen, S.J., Li, Z. and Zhang, J.S. (2016), "Research on hysteretic performance of steel reinforced concrete T-shaped column", *In MATEC Web of Conferences*.

Zhou, T., Chen, Z.H. and Liu, H.B. (2012), "Seismic behavior of special-shaped column composed of filled steel tubes", *J. Constr. Steel Res.*, **75**, 131-141.

CC